Journal of Alloys and Compounds 509 (2011) 3917–3923

Contents lists available at ScienceDirect

Journal of Alloys and Compounds

journal homepage: www.elsevier.com/locate/jallcom

Structural, magnetic and electrical properties of nanocrystalline zinc ferrite

A. Pradeep[a,*], P. Priyadharsini[b], G. Chandrasekaran[b]

[a] Department of Physics, Periyar Arts College, Cuddalore 607 001, India
[b] Department of Physics, School of Physical, Chemical and Applied Sciences, Pondicherry University, Puducherry 605 014, India

ARTICLE INFO

Article history:
Received 18 August 2010
Received in revised form
20 December 2010
Accepted 22 December 2010
Available online 30 December 2010

Keywords:
$ZnFe_2O_4$ nanoparticles
Sol–gel
Structural property
Magnetic property
Electrical property

ABSTRACT

Nanoparticles of $ZnFe_2O_4$ with grain size of 30 nm have been synthesized via sol–gel auto combustion method and characterized using DSC (differential scanning calorimetry), XRD (X-ray diffraction), SEM (scanning electron microscopy), EDAX (energy dispersive X-ray analysis), FTIR (Fourier transform infrared spectroscopy), VSM (vibrating sample magnetometer) and Ac-electrical conductivity measurement setup. Structural analysis using XRD and FTIR show the formation of spinel structure in nano $ZnFe_2O_4$ particles. The cation distribution in the sample has been estimated theoretically and the results show that as-prepared nanoparticles of $ZnFe_2O_4$ have partially inverted ionic distribution in comparison with that of bulk zinc ferrite. Results from EDAX indicate the ratio of Fe:Zn as close to 2:1. The presence of a weak ferrimagnetic phase for nano $ZnFe_2O_4$ at room temperature has been established from its hysteresis behavior. Redistribution of cations occurring at nano-regime and surface spin canting of nanoparticles of $ZnFe_2O_4$ are expected to be responsible for the presence of magnetic ordering in nano $ZnFe_2O_4$. The Curie temperature of nano $ZnFe_2O_4$ determined from magnetization versus temperature measurement is equal to 375 °C. The electrical conductivity of the present $ZnFe_2O_4$ at a frequency of 100 kHz at room temperature is observed to be $2.11 \times 10^{-8}\ \Omega^{-1}\ cm^{-1}$ which is four orders lesser in magnitude than the value of bulk $ZnFe_2O_4$. Overall conductivity response with respect to temperature and frequency confirm that $ZnFe_2O_4$ tends to become more dielectric in the nano-regime.

1. Introduction

Ferrites in nano scale dimension show fascinating and unusual properties compared to their bulk counterparts. The applications of ferrites are growing in leaps and bounds with the advancement in nanotechnology. The study of nano structured zinc ferrite has been receiving increased attention amongst material scientists in recent years. Zinc ferrite has been used as an adsorbent material for hot-gas desulfurization [1,2] and for the elimination of other toxic gases like H_2S, CO_2 and NO from coal gas [3]. $ZnFe_2O_4$ is reported to be a potential candidate for application as photocatalyst [4]. Bulk $ZnFe_2O_4$ is a normal spinel with all the Zn ions occupying tetrahedral sites and Fe^{3+} ions occupying octahedral sites [5]. Magnetic studies on bulk $ZnFe_2O_4$ showed the presence of strong paramagnetic phase at room temperature and a weak antiferromagnetic ordering below its Neel's temperature which is around 10 K [6,7]. But recent investigations [8–10] on nanoparticles of zinc ferrite report the presence of ferrimagnetic ordering at room temperature. This change in magnetic ordering is due to the redistribution or inversion of cations between the tetrahedral and octahedral sites. The migration of Fe^{3+} ions to the tetrahedral sites results in net magnetization due to the A–O–B superexchange mechanism. Thus the properties exhibited by $ZnFe_2O_4$ are likely to change with the particle size and inversion of cations in the sites. The inversion parameter in turn is dependent on the route of synthesis. Nanoscale $ZnFe_2O_4$ exhibiting ferrimagnetic behavior has been synthesized using various methods including ball milling [8], combustion synthesis [9], co-precipitation [10] and thin film technology [11]. This work is an attempt to synthesize $ZnFe_2O_4$ using sol–gel citrate–nitrate route and to study its structure, magnetic properties and electrical conductivity in the limit of nano-regime. Sol–gel method is a simple, cost-effective and reliable low temperature technique for the preparation of nano ferrites. Moreover, it offers good control over the stoichiometric composition and the microstructure of the desired product.

2. Experimental

Nanoparticles of $ZnFe_2O_4$ have been prepared by sol–gel auto combustion method. Analytical grade $Zn(NO_3)_2{\cdot}6H_2O$ and $Fe(NO_3)_3{\cdot}9H_2O$ are mixed with citric acid. The ratio of the nitrates to citric acid is 1:1. The slurry mixture is then dissolved in 200 ml of deionized water. Citric acid helps for the homogenous distribution and segregation of the metal ions. Small amount of ammonium hydroxide is added carefully to the solution to change the pH value to 7. The solution is then continuously stirred using a magnetic stirrer. Condensation reaction occurs

* Corresponding author. Tel.: +91 9787057007.
E-mail address: arumugampradeep@yahoo.com (A. Pradeep).

0925-8388/$ – see front matter © 2011 Elsevier B.V. All rights reserved.
doi:10.1016/j.jallcom.2010.12.168

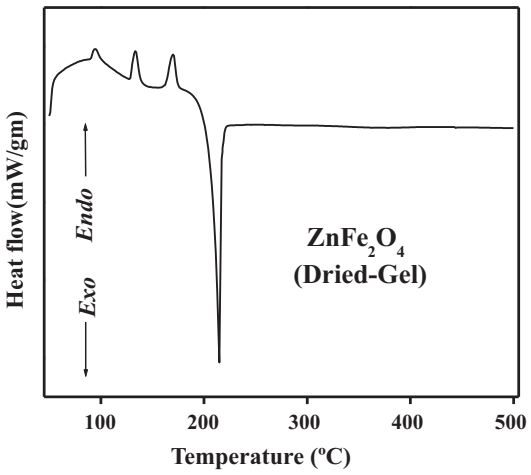

Fig. 1. Thermal behavior of dried-gel precursor of $ZnFe_2O_4$.

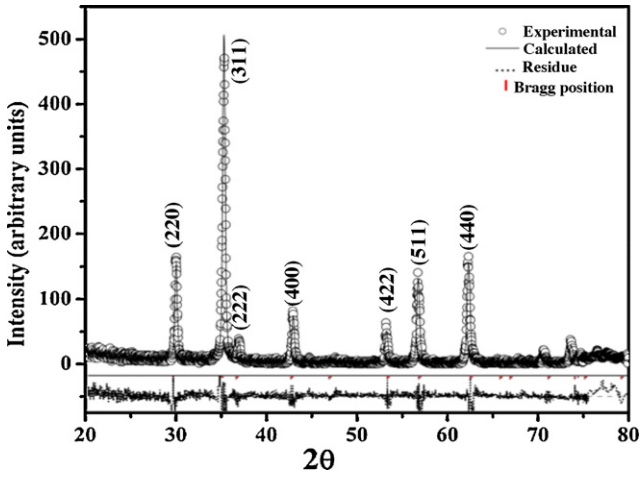

Fig. 2. XRD pattern of as-prepared $ZnFe_2O_4$ powder synthesized using sol–gel route.

between adjacent metal nitrates and molecules of citric acid and forms a polymer like network which then grows into colloidal dimensions known as sol. The resultant sol is poured in a silica crucible and heated at 135 °C under constant stirring to transform into xerogel or dried gel. Continuous heating leads to the formation of nano powder of Zn-ferrite through a self-propagating combustion process. Thermal behavior of dried gel precursor has been studied using DSC (METTLER TOLEDO STAR^e System (Model: DSC 821^e)). Phase identification of the as-prepared powder of $ZnFe_2O_4$ has been done using XRD (PANalytical (Model: X'Pert PRO)). The structural morphology and elemental composition have been investigated using SEM–EDAX (HITACHI (Model: S-3400N)). Infrared study of the as-prepared powder of zinc ferrite has been done using FTIR instrument (SHIMADZU (Model: 8700)). Magnetic studies at room temperature have been carried out using VSM (LAKESHORE (Model: 7404)). Ac-conductivity measurements have been made using ZENTECH (3305 automatic component analyzer) meter. The as-prepared $ZnFe_2O_4$ powder is made into 'GREEN' pellets (thickness = 3 mm and diameter = 13 mm) using a hydraulic press (SPECTRALAB) under a pressure of 80 kg/cm^2. The surfaces of pellets are polished carefully to be parallel and smooth. Connection leads are made using very short copper wires with silver paste as a contact material. Conductance G_p and capacitance C_p are measured as a function of frequency range from 100 Hz to 1 MHz for a fixed temperature. The above procedure is repeated for different temperatures (from RT to 500 °C in steps of 50 °C). Conductivity values are obtained from the observed conductance, thickness and area of the pellet.

3. Results and discussion

3.1. Formation of ferrite and phase analysis

DSC study of dried gel precursor has been carried out in order to understand the change of phases occurring during the synthesis of zinc ferrite. Generally the precipitation of phases, recovery and re-crystallization reactions are exothermic, while second-phase dissolution reactions are endothermic [12]. The DSC curve of the dried-gel precursor of $ZnFe_2O_4$ is shown in Fig. 1.

The DSC curve shows two notable endothermic peaks at 133 °C and 168 °C. They are due to the vaporization of planar and locked-in water molecules, respectively, present in the dried gel [13]. A sharp and intense peak at 214 °C represents the auto-combustion process liberating enormous heat to form well crystallized $ZnFe_2O_4$. The crystallization of ferrite material is thus achieved in a single step which sanctifies the preference of this method compared to other low temperature methods.

The XRD pattern of the as-prepared $ZnFe_2O_4$ powder synthesized using sol–gel method is shown in Fig. 2. It shows the presence of diffraction peaks corresponding to spinel ferrite structure. A close scrutiny of the pattern reveals the presence of well defined, sharp and intense peaks which confirms that the $ZnFe_2O_4$ sample has crystallized well. Reitveld analysis of the XRD data has been carried out by fitting pseudo-voigt profile in size-strain mode using PANalytical X-pert Highscore Plus software. The refined values of lattice constant (a), grain size (t) and microstrain (ε) are as follows: $a = 8.429$ Å ($R_{exp} = 27.3$, $R_p = 24.2$, $R_{wp} = 34.7$, $\chi^2 = 1.6$), $t = 28$ nm and $\varepsilon = 0.012\%$. The grain size of nano Zn ferrite is also estimated using Scherrer's equation and is found to be around 30 nm [14]. The FWHM value of the peak corresponding to (3 1 1) plane was considered for this purpose after correction for instrumental broadening. Thus the sol–gel citrate nitrate route has been successful in yielding single phase nanoparticles of $ZnFe_2O_4$.

Using the ionic size data of the respective ions [15], the cation distribution has been estimated theoretically with reference to the refined lattice constant value using the following formula proposed by Bhongale et al. [16].

$$a = \frac{\{(r_a/\sqrt{3} + r_b + 2.0951r_o) + [(r_a/\sqrt{3} + r_b + 2.0951r_o)^2 - 1.866(1.333r_a^2 + 0.0675r_o^2 - 0.6r_a r_o)]^{1/2}\}}{1.106} \quad (1)$$

where r_a and r_b are the radii of the ions present in A-site and B-site, respectively, whereas r_o is the ionic radius of oxygen. An indigenous computer program in FORTRAN-77 has been developed to determine the cation distribution in ferrites. Amongst the various possible distributions, the one which fits well with the experimental lattice constant value and also compatible for explaining its magnetic property is chosen. The proposed cation distribution for the present nano Zn-ferrite is as follows: $(Zn^{2+}_{0.65}Fe^{3+}_{0.35})_A[Zn^{2+}_{0.35}Fe^{3+}_{1.43}Fe^{2+}_{0.22}]_B$. The cation distribution shows that Zn^{2+} ions which otherwise have high tetrahedral site preference energy have occupied the octahedral site to a significant amount. It is also seen that a considerable amount of Fe^{3+} ions have migrated in lieu of Zn^{2+} ions to A-site. The relative inversion of cations and the decrease in lattice constant value compared to bulk Zn ferrite is attributable as an outcome of the intermediary processes involved in the route of synthesis. Latest reports claim that redistribution of cations takes place in nanoparticles of $ZnFe_2O_4$ and the amount of inversion depends on the grain size and route of synthesis. Akhtar et al. [17] have prepared nano $ZnFe_2O_4$ by sol–gel method using citric acid as the fuel. They have reported cation distribution equal to $(Zn^{2+}_{0.75}Fe^{3+}_{0.25})_A[Zn^{2+}_{0.25}Fe^{3+}_{1.75}]_B$ for a grain size of 18nm. This distribution closely matches with the present work let alone the presence of Fe^{2+} ions in our distribution.The FTIR spectrum of as-prepared powder of $ZnFe_2O_4$ is shown in Fig. 3. The FTIR spectrum shows two persistent absorption bands character-

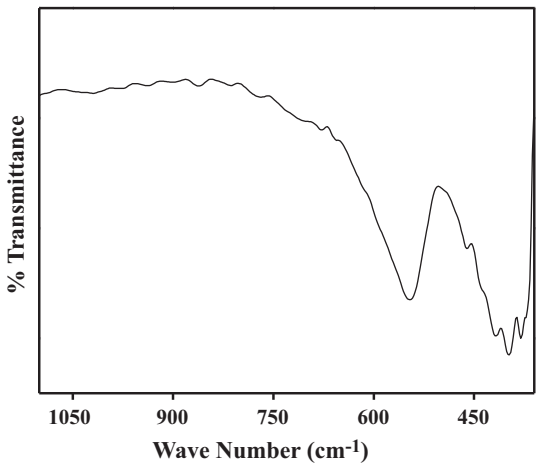

Fig. 3. FTIR spectrum of as-prepared powder of nano $ZnFe_2O_4$.

istic of spinel structure at frequencies $\upsilon_1 = 545$ and $\upsilon_2 = 392\,cm^{-1}$ corresponding to the vibration of the oxygen–metal cation complexes present in the tetrahedral and octahedral sites, respectively. The spectrum also reveals the presence of a broad shoulder for tetrahedral site and subsidiary bands at the octahedral site. The presence of broad shoulder along with the subsidiary bands are attributed to the presence of cations with different ionic states in both the sites. This is mainly due to the encroachment of Zn^{2+} ions to B-site and subsequent shifting of Fe^{3+} ions to the A-site. The absorption bands of the present nano Zn-ferrite system have shifted to lower frequencies when compared to bulk $ZnFe_2O_4$ [18]. It is a well-known fact that the bondlength and vibrational frequency are inversely proportional. The redistribution of the cations results in change in the bond length of cation–oxygen complexes in the interstitial sites which eventually explains the change in vibrational frequency of the absorption bands. The observation from FTIR study supports the explanation given using XRD study for the inversion of Zn and Fe leading to mixed cation distribution.

3.2. Structural morphology and chemical composition

The structural morphology of the as-synthesized powder is investigated using SEM. The SEM micrographs of the as-synthesized $ZnFe_2O_4$ for a resolution of 10 μm and 3 μm are shown in Fig. 4(a and b).The micrographs show rounded clusters of particles of uniform sizes. It is seen from Fig. 4b that the size of one of the agglomerated cluster of particles is around 243 nm which is greater than the grain size estimated from XRD data. This is indicative of the fact that every particle is formed by a number of crystallites or grains.

Energy dispersive X-ray analysis is carried out in order to verify the elemental composition and to test the presence of impurities if any present in the sample. The EDAX spectrum of the nano $ZnFe_2O_4$ is shown in Fig. 5. The percentage of atoms reported using the spectrum shows Fe:Zn ratio close to 2:1. The spectrum shows the different orbital states of only Zn, Fe and O which certifies that the sample is devoid of any magnetic impurity state other than Fe.

3.3. Magnetic study

Magnetization measurements are finger print proofs for investigating the magnetic ordering present in a magnetic material. The as-prepared $ZnFe_2O_4$ powder shows distinct hysteresis loop at room temperature for a maximum applied field of 10 kG. It is seen that hysteresis loop of nano $ZnFe_2O_4$ shown in Fig. 6 does not

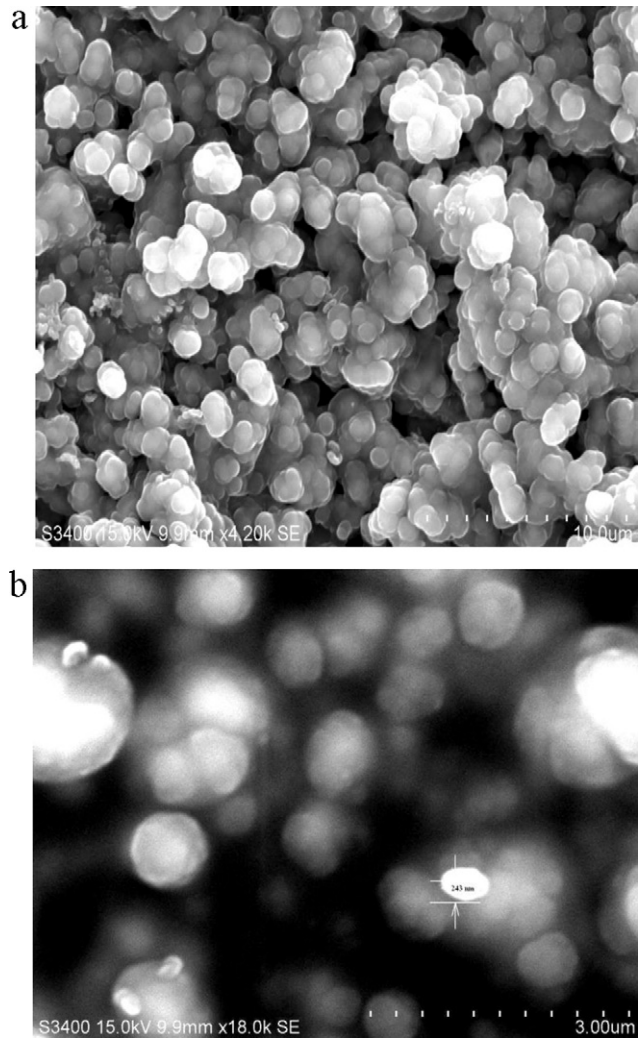

Fig. 4. (a and b) SEM micrographs of the as-prepared powder of $ZnFe_2O_4$.

saturate even at the maximum applied field. Saturation magnetization (M_s) for the sample is obtained by fitting the high field curve to the function $M_s = M(1 - \alpha/H)$, where α is a fitting constant, and H is the applied magnetic field. Nanoparticles of $ZnFe_2O_4$ are thus found to exhibit hysteresis behavior quite contradictory to its bulk counterpart. This is clearly a magnetic effect of nano regime and not because of any magnetic moment bearing impurity phase which is confirmed through EDAX analysis of the sample.

The hysteresis behavior in nano $ZnFe_2O_4$ compared to bulk $ZnFe_2O_4$ is explained to be primarily arising from the following two mechanisms:

(1) Redistribution of cations between tetrahedral and octahedral sites.
(2) Spin canting component from large fraction of particles present in the surface of nano $ZnFe_2O_4$.

The redistribution of cations in nano $ZnFe_2O_4$ can be explained in the light of cation distribution proposed using XRD data. Bulk $ZnFe_2O_4$ is a normal spinel where Zn ions occupy A-site and Fe ions strictly occupy B sites. Since non magnetic Zn ions occupy A-site the resultant magnetic moment is largely due to weak antiferromagnetic exchange interactions between magnetic Fe–Fe ions in the B-site. Therefore, bulk $ZnFe_2O_4$ possesses near zero moment at room temperature. According to the cation distribution of the

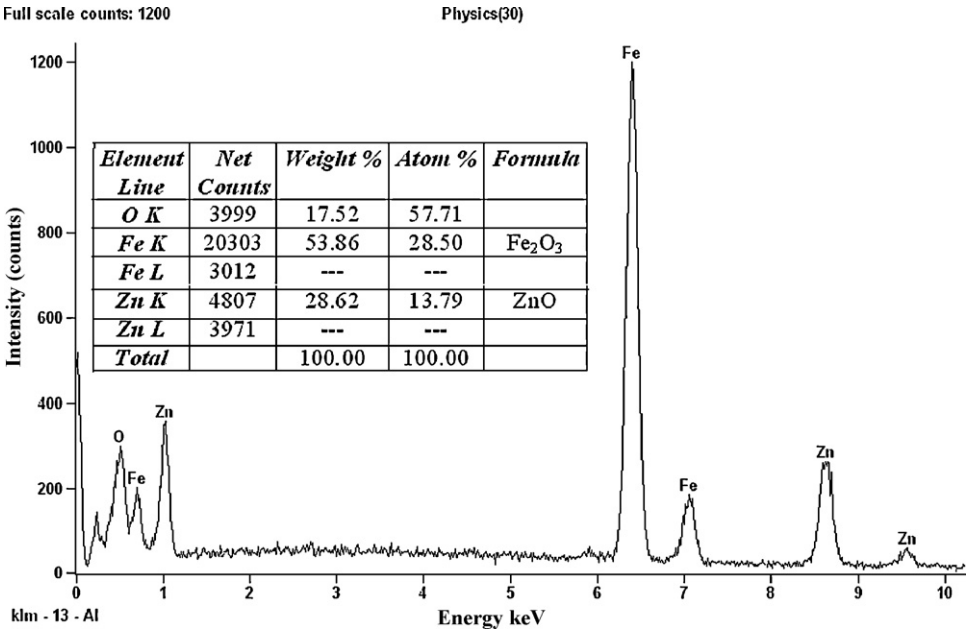

Element Line	Net Counts	Weight %	Atom %	Formula
O K	3999	17.52	57.71	
Fe K	20303	53.86	28.50	Fe_2O_3
Fe L	3012	---	---	
Zn K	4807	28.62	13.79	ZnO
Zn L	3971	---	---	
Total		100.00	100.00	

Fig. 5. EDAX spectrum of as-prepared $ZnFe_2O_4$ powder.

present $ZnFe_2O_4$ sample, the Fe^{3+} ions are found to occupy both A- and B-sites. Therefore, Fe–Fe interaction between A–B sublattices dominates and is much stronger than Fe–Fe ions interaction in the B site. A ferrimagnetic or uncompensated moment arises from this A–B exchange interaction due to the unequal number of Fe^{3+} ions on the two types of sites and this largely enhances saturation magnetization in nano $ZnFe_2O_4$ [19,20]. Thus the exchange effect between Fe^{3+} ions in both the sites is accountable for the observation of hysteresis loop at room temperature.

The present $ZnFe_2O_4$ sample with grain size 30 nm is found to exhibit a saturation magnetization value equal to 7.8 emu/g, a high value of coercive force equal to 128 G and a remanent magnetization equal to 0.83 emu/g. The order of the value of magnetization, coercive field and ratio of remanence to magnetization at high field are all indicative of formation of domains and setting in of ferrimagnetic phase in the sample. The ferrimagnetic behavior of nano Zn-ferrite has been observed by Chinnasamy et al. [8,21,22], Jun Wang et al. [23] and Oliver et al. [24]. Further evidences for the presence of Zn^{2+} in B-site and Fe^{3+} in A-site has been reported earlier by Jeyadevan et al. [25] through EXAFS studies and Lotgering [19] through neutron diffraction studies. Misra et al. [26] have reported a magnetization value of 6 emu/g for 8 nm particles of $ZnFe_2O_4$. Shenoy et al. [10] prepared nano $ZnFe_2O_4$ using a less common co-precipitation technique followed by ball-milling and found saturation magnetization around 7.5 emu/g for a particle size of 9 nm. Chinnasamy et al. [21] have synthesized $ZnFe_2O_4$ particles of different sizes using high-energy ball-milling and has reported magnetization value around 4.5 emu/g for a particle size of 22 nm. Animesh Kundu et al. [27] have reported magnetization value equal to 21 emu/g for a particle size of 13 nm. The difference in the values of saturation magnetization suggests that M_s values are strongly dependent on the inversion parameter which is in turn dependent on the method of synthesis.

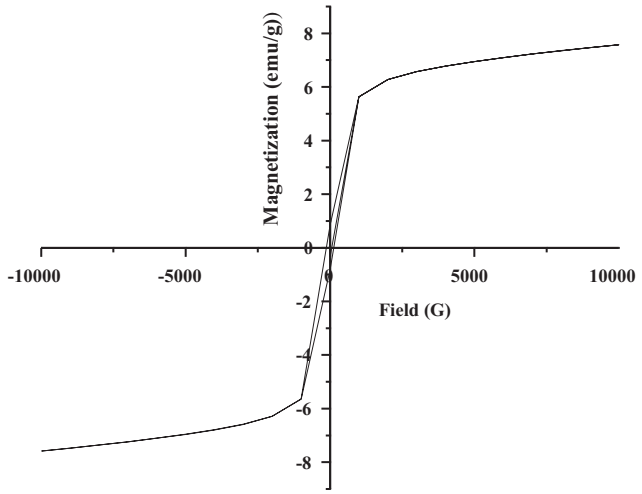

Fig. 6. Hysteresis loop of as-prepared $ZnFe_2O_4$ at 300 K.

The resultant magnetic moment observed is also due to spin canting of $ZnFe_2O_4$ nanoparticles where fraction of the total spins at the surface will have a non-collinear configuration with respect to the core ones, due to broken exchange bonds and symmetry. Moreover, the non-saturation of hysteresis loop at 10 kG is suggestive of the presence of spin disorder in the surface of $ZnFe_2O_4$. The spin disorder at the surface may be related to spin canting and is explained by means of core–shell model which is basically two-component nanoparticles system consisting of a spin-glass like surface layer and ferrimagnetically aligned core spins coupled by exchange interactions [28]. With the increase in magnetic field, the core magnetic moments start to align along the applied field. After all the core moments are completely aligned the contribution from core magnetic moments get exhausted and the magnetization response is saturated in a usual Langevin-like way. Any increase in the magnetic field thereafter affects only surface layer of the particles and thus the increase in the magnetization of the particles slow down. This leads to a virtual absence of magnetic saturation that keeps the hysteresis loops unsaturated even in very strong fields.

The value of experimental magnetic moment (μB) is determined using M_s value and is found to be equal to 0.327 μB [29]. According to Neel's double lattice model it can be explained that the presence of Fe^{3+} ions on both A and B-sites in different proportions is responsible for a finite value of the observed magnetic moment. The theoretically calculated value of magnetic moment by Neel's theory is 0.8 μB. The deviation is attributed as the effect of canted

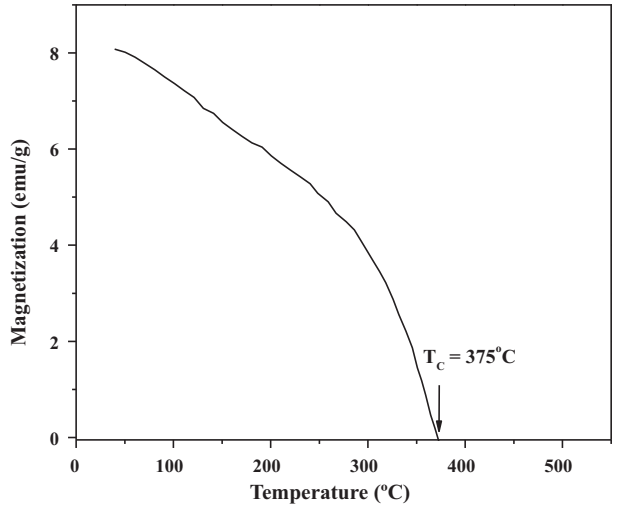

Fig. 7. Temperature dependent magnetization behavior of nano$ZnFe_2O_4$.

or triangular lattice arrangement of magnetic moments. Using the triangular lattice of moments the value of canting angle or Y–K angle is calculated for scientific interest and is equal to 54°62′. The reported value of spin canting angle for bulk Zn ferrite is equal to 90° [30]. The lowering of the canting angle is an effective contribution of nanoregime. Thus it is evident that spin canting is also the cause for the deviation between and observed and theoretical values of magnetic moment in the nano Zn-ferrite. We predict that spin canting is predominantly found in B site although more specific investigation like Mossbauer study is needed to confirm that.

Fig. 7 shows the change in magnetization of nano $ZnFe_2O_4$ particles as a function of temperature in an applied magnetic field of 10 kG. It is seen from Fig. 7 that there is a gradual decrease in magnetization with temperature up to 325 °C after which there is quite a sharp fall in the magnetization until it becomes zero at 375 °C. It is explained that the thermal energy helps the metal ions to overcome the energy barriers preventing an ordered cation distribution. Hence the inversion parameter decreases which results in the weakening of A–B exchange interaction. Therefore, there is a fall in the magnetization value. It can be understood that the tendency to become normal spinel is more after 325 °C. The Curie temperature of the material is around 375 °C (648 K) after which the material behaves like a paramagnet. There are widely scattered values of the Curie temperature of zinc ferrite in the literature. Deka and Joy [31] have reported a T_c value equal to 800 K whereas Chen et al. [32] reported a T_c value close to 600 K for thin film of zinc ferrite. It appears that the transition temperature of $ZnFe_2O_4$ may vary depending on sample processing conditions and the synthesis methods.

3.4. Analysis of Ac-conductivity data of nano $ZnFe_2O_4$

3.4.1. Dielectric behavior

The dielectric properties of ferrites depend on several factors, including the method of synthesis, grain size and chemical composition. The dependence of complex permittivity of nano $ZnFe_2O_4$ with respect to frequency at different temperatures is studied. The frequency dependence of real and imaginary parts (ε' and ε'') of dielectric permittivity at different temperatures are shown in Fig. 7(a and b). It is seen from Fig. 8(a and b) that there is a monotonous decrease in the values of ε' and ε'' with increasing frequency. The observed trends can be explained using the idea of

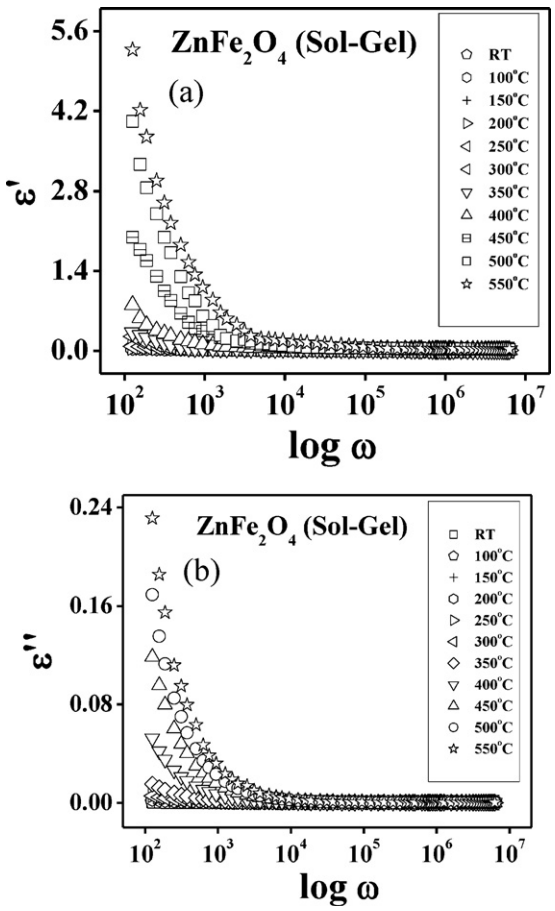

Fig. 8. (a and b) Plots of real (ε') imaginary (ε'') parts of dielectric constant versus frequency at different temperatures.

interfacial polarization suggested by Koops [33]. Ferrites are dipolar materials due to the presence of majority Fe^{3+} ions and minority Fe^{2+} ions in them. Fe^{2+} ions are usually formed due to partial reduction of Fe^{3+} ions during the process of synthesis. The electron exchange between Fe^{3+} and Fe^{2+} ions gives local displacement of electrons in the direction of applied electric field thus inducing polarization in ferrites. The decrease in the complex permittivity with increasing frequency is explained to be due to the decrease of polarization of the dipoles when electric field propagates with high frequency. In other words beyond a certain frequency or electric field the electron exchange does not follow the alternating field. It is also noticed from Fig. 8(a and b) that the polarization increases with the increase in temperature. It is explained to be due to thermal activation which enhances the number of dipoles available for polarization when the sample is at a high temperature. At high temperatures an exponential decrease of (ε' and ε'') with respect to frequency is observed whereas complex permittivity is almost frequency independent at low temperatures.

A plot of dielectric loss tangent ($\tan\delta$) versus temperature at different frequencies is shown in Fig. 9. It is observed that $\tan\delta$ shows an increasing trend with rise in temperature. It is seen that at temperatures less than 200 °C, the dielectric loss is very low and found to be frequency independent. The value of $\tan\delta$ measures the loss of electrical energy incurred by the electric field at different frequencies. The loss of electrical field is more at high frequency because of increase in interruption to the passage of electric field through the sample due to the interaction of it with the oscillating majority charges carriers of the dipoles.

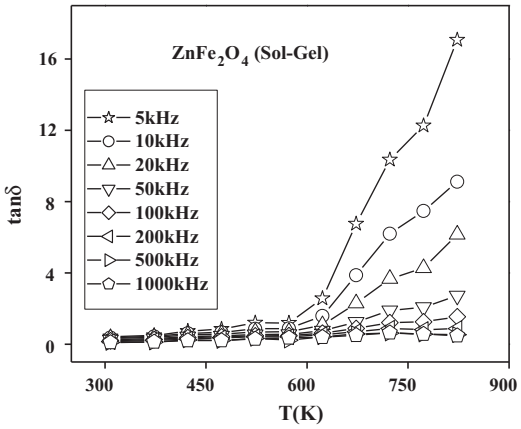

Fig. 9. Variation of dielectric loss tangent (tan δ) with frequency of nano $ZnFe_2O_4$ at different temperatures.

3.4.2. Frequency dependence of Ac-conductivity

The values of electrical conductivity of the nano zinc ferrite are plotted against the change in frequency for different temperatures and shown in Fig. 10. It is seen that the conductivity of Zn-ferrite shows a gradual rise at low frequencies whereas at higher frequencies the conductivity rises steeply. The trend can be explained as follows: at low frequencies the conductivity is low due to grain boundary effect which acts as hindrance for mobility of the charge carriers. At high frequency regions the conductivity is mainly due to the ionic part which masks the effect due to grain boundaries. The trend is similar to that of variation of tan δ with respect to frequency. At high temperatures the conductivity rises very gradually with the frequency, i.e. the frequency has very little effect on the thermally activated charge carriers and the conductivity is mainly due to the band conduction mechanism. The conduction mechanism suggested for $ZnFe_2O_4$ is the electron hopping between the bands, i.e. $Fe^{3+} \Leftrightarrow Fe^{3+} + e^-$.

The reciprocal behavior of conductivity with respect to permittivity goes hand in hand for the semiconductor behavior of the ferrite under study. Moreover, conductivity and tan δ (Figs. 9 and 10) show similar trend with reference to frequency. It is likely that the mechanism would be the interruption or interaction of electric field with the free electrons of the localized bands. When the electric field is passing at high frequency it has high probability of interacting with the electrons.

3.4.3. Temperature dependence of Ac-conductivity

The reports on the Ac-conductivity of nano sized $ZnFe_2O_4$ are scanty in the literature. Ponpandian and Narayanasamy [34] have

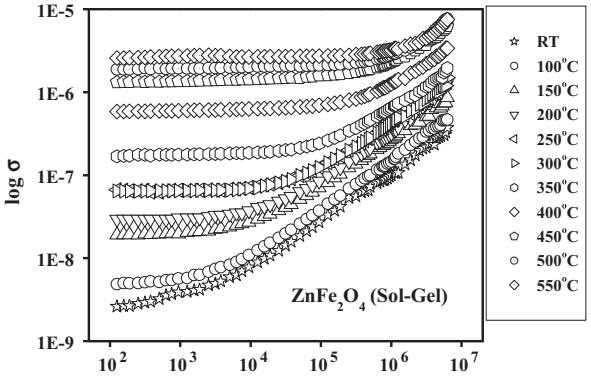

Fig. 10. Frequency dependent Ac-conductivity behavior of nano $ZnFe_2O_4$ at different temperatures.

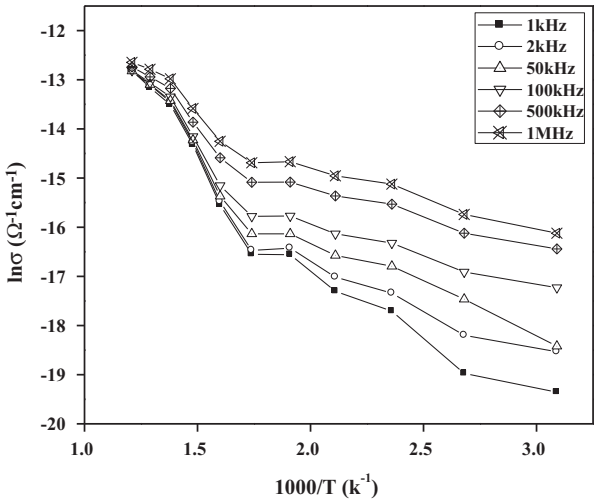

Fig. 11. Temperature dependent Ac-conductivity behavior of nano $ZnFe_2O_4$ at different frequencies.

studied the influence of grain size on the electrical properties of nanocrystalline $ZnFe_2O_4$. In the present work the variation of Ac-electrical conductivity of $ZnFe_2O_4$ with temperature at selected frequencies is shown in Fig. 11. It is seen from Fig. 11 that the conductivity increases with the increase in temperature which is a typical behavior of semiconductors. A close scrutiny of the curves shows that there is a change of slope at all frequencies after a particular temperature, i.e. 350°. It is worthy to note that the value of conductivity makes a sudden spurt to higher values at high temperatures. This calls for the possibility of two different types of conduction mechanism in this ferrite. Accordingly, the conductivity behavior can be split into two temperature zones as follows: (1) RT–350 °C and (2) 350–550 °C. It has been established in the magnetic study that $ZnFe_2O_4$ of the present study possesses ferrimagnetic phase with Curie temperature equal to 375 °C. In the light of that information it is explained that the first temperature zone corresponds to the ferrimagnetic ordering region whereas the second zone corresponds to the paramagnetic region of the nano Zn-ferrite. Figueroa and Stewart [35] have investigated the thermal evolution of the non-equilibrium state in nano-sized $ZnFe_2O_4$. They have reported that cationic inversion does not change until the activation barrier is overcome at $T_a = 585$ K. Above T_a, the Zn ions continuously change their environment to their normal equilibrium state and the room-temperature magnetic state changes from ferrimagnetic to paramagnetic. Mozaffari et al. [36] have also reported a decrease in the degree of inversion with increasing temperature in nano $ZnFe_2O_4$. In that case we may very well say that the temperature to overcome activation barrier is very close to the Curie temperature of our sample. The trend in which conductivity changes with temperature explains that the ferrimagnetic exchange interaction hinders conduction mechanism whereas the paramagnetic phase due to the absence of exchange interaction supports conduction mechanism. The magnetic coupling of conduction electrons of localized bands is the main cause for reducing the conductivity. The increase in electrical conductivity as the temperature rises would be attributed to the absence of magnetic coupling which enhances the drift mobility of the thermally activated charge carriers (hopping mechanism). The conductivity of the ferrite varies with temperature according to the Arrhenius equation

$$\sigma = \sigma_0 \exp\left(\frac{\Delta E}{kT}\right) \quad (2)$$

where k is the Boltzmann's constant, ΔE is the activation energy (eV) and T is the temperature (K). The slope of the $\ln \sigma'$ versus

1000/T straight line is a measure of activation energy (ΔE) of the ferrite.

The values of activation energy at a frequency of 100 kHz for the present nano $ZnFe_2O_4$ is equal to 0.41 eV in the ferrimagnetic region and 0.65 eV in the paramagnetic region. The electrical conductivity of the present $ZnFe_2O_4$ at a frequency of 100 kHz at room temperature is observed to be $2.11 \times 10^{-8}\ \Omega^{-1}\ cm^{-1}$. Satyanarayana et al. [37] has reported the value of conductivity equal to $3.88 \times 10^{-4}\ \Omega^{-1}\ cm^{-1}$ for bulk $ZnFe_2O_4$ under similar conditions. It is seen that the value of Ac-conductivity has reduced by an order of four in magnitude for the Zn-ferrite under study. It is attributable to the impact of nanosize of the particles causing band gap widening as well as the magnetic coupling caused by the exchange interaction of ferrimagnetism on the hopping electrons of localized bands. It is attributed as a result of nanograins of Zn ferrite becoming more dielectric and also due to the hindrance offered by magnetically polarized electrons in the bands. A suitable explanation can be provided considering the distribution of ions in tetrahedral and octahedral sites. The main cause for the conductivity mechanism in ferrite can be due to e^- hopping between Fe^{2+} and Fe^{3+} ions present in the octahedral sites, i.e. $Fe^{2+} \Leftrightarrow Fe^{3+} + e^-$ [38]. It is explained on the basis of the order of the activation energy of the present ferrite that the higher value of activation energy corresponds to exciton/polaron activated hopping and the lower value of it is due to electron hopping between localized bands of the paramagnetic and ferrimagnetic phase, respectively. The change of slope at a particular temperature and activation energy at low and high temperatures as well as conductivity clearly establish the fact that the drift of conduction electrons of electrical conducting mechanism is hindered by the presence ferrimagnetic phase in the material.

4. Conclusion

Nanoparticles of $ZnFe_2O_4$ showing ferrimagnetic behavior at room temperature have been successfully synthesized by sol–gel auto combustion route. The enormous heat liberated during the combustion process has played a significant role in the inversion of distribution of cations. The DSC, XRD and FTIR data support the above argument. The prepared sample is found to possess good stoichiometric composition which is an added advantage compared to other preparation techniques. The magnetic study shows the ferrimagnetic behavior of nano Zn-ferrite characterized with relatively high saturation magnetization and coercivity values which can be of immense use in memory device applications. The Curie temperature estimated using magnetic and study confirm the ferrimagnetic phase of nano Zn ferrite. Furthermore, conductivity studies show that the ferrimagnetic exchange interaction hinders conduction mechanism whereas the paramagnetic phase of $ZnFe_2O_4$ supports conduction mechanism due to the absence of exchange interaction. The electrical study shows a decrease in conductivity when compared to bulk Zn ferrite which explains the dielectric nature of the $ZnFe_2O_4$ when prepared as nanoparticles. It is concluded that Zn ferrite in nanograins is further interesting as it is influenced by magnetic coupling between hopping electrons which needs scrupulous investigation.

Acknowledgements

The authors thank, DST-FIST, Govt. of India for funding the facilities utilized in the present investigation in the Department of Physics and Central Instrumentation Facility of Pondicherry University. The authors also thank Prof. G. Govindaraj, Dept. of Physics, Pondicherry University for his kind permission to use Ac-conductivity bridge. One of the authors (P. Priyadharsini) thanks the CSIR, India for the award of Senior Research Fellowship (No. 09/559/(0056)/2009/EMR-I dated 23-4-2009).

References

[1] R.E. Ayala, D.W. Marsh, Ind. Eng. Chem. Res. 30 (1991) 55–60.
[2] L.A. Bissett, L.D. Strickland, Ind. Eng. Chem. Res. 30 (1991) 170–176.
[3] F.A. Lopez, A. Lopez-Delgado, J.L. Martin de Vidales, E. Vila, J. Alloys Compd. 265 (1998) 291–296.
[4] Hun Xue, Zhaohui Li, Xuxu Wang, Xiangzhi Fu, Mater. Lett. 61 (2007) 347–350.
[5] G.F. Goya, H.R. Rechenberg, J. Magn. Magn. Mater. 203 (1999) 141–142.
[6] F.S. Li, L. Wang, J.B. Wang, Q.G. Zhou, X.Z. Zhou, H.P. Kunkel, G. William, J. Magn. Magn. Mater. 268 (2004) 332–339.
[7] L.D. Tung, V. Kolesnichenko, G. Caruntu, D. Caruntu, Y. Remond, V.O. Golub, C.J. O'Connor, L. Spinu, Physica B 319 (2002) 116–121.
[8] C.N. Chinnasamy, A. Narayanasamy, N. Ponpandian, K. Chattopadhyay, H. Guérault, J.M. Greneche, Scripta Mater. 44 (2001) 1407–1410.
[9] M.K. Roy, Bidyut Haldar, H.C. Verma, Nanotechnology 17 (2006) 232–237.
[10] S.D. Shenoy, P.A. Joy, M.R. Anantharaman, J. Magn. Magn. Mater. 269 (2004) 217–226.
[11] M. Bohra, S. Prasad, N. Kumar, S.C. Sahoo, D.S. Mishra, N. Venkataramani, R. Krishnan, Appl. Phys. Lett. 88 (2006) 262506–262513.
[12] Chung-Min Chang, J.G. Byrne, Mater. Sci. Eng. A 60 (1993) 91–100.
[13] Yujie Huang, Yan Tang, Jun Wang, Qianwang Chen, Mater. Chem. Phys. 97 (2006) 394–397.
[14] H. Klung, L. Alexander, X-ray Diffraction Procedures, Wiley, New York, 1962, p. 491.
[15] CRC Handbook of Chemistry and Physics, Internet Version, 2005.
[16] G.M. Bhongale, D.K. Kulkarni, V.B. Sapre, Bull. Mater. Sci. 15 (1992) 121–125.
[17] M.J. Akhtar, M. Nadeem, S. Javaid, M. Atif, J. Phys.: Condens. Matter 21 (2009) 405303–405309.
[18] R.D. Waldron, Phys. Rev. 99 (1955) 1727–1735.
[19] F.K. Lotgering, J. Phys. Chem. Solids 27 (1966) 139–145.
[20] M. Atif, S.K. Hasanain, M. Nadeem, Solid State Commun. 138 (2006) 416–421.
[21] C.N. Chinnasamy, A. Narayanasamy, N. Ponpandian, K. Chattopadhyay, H. Guérault, J.M. Greneche, J. Phys.: Condens. Matter 12 (2000) 7795–7805.
[22] C.N. Chinnasamy, A. Narayanasamy, N. Ponpandian, K. Chattopadhyay, Mater. Sci. Eng. A 304 (2001) 983–987.
[23] Jun Wang, Chuan Zeng, Zhenmeng Peng, Qianwang Chen, Physica B 349 (2004) 124–128.
[24] S.A. Oliver, H.H. Hamdeh, J.C. Ho, Phys. Rev. B 60 (1999) 3400–3405.
[25] B. Jeyadevan, B. Tohiji, K. Nakatsuka, J. Appl. Phys. 76 (1994) 6325–6333.
[26] R.D.K. Misra, S. Gubbala, A. Kale, W.F. Egelhoff Jr., Mater. Sci. Eng. B 111 (2004) 164–174.
[27] Animesh Kundu, C. Upadhyay, H.C. Verma, Phys. Lett. A 311 (2003) 410–415.
[28] R.H. Kodama, A.E. Berkowitz, E.J. McNiff, S. Foner, Phys. Rev. Lett. 77 (1996) 394–397.
[29] J. Smit, H.P.J. Wijn, Ferrites, vol. 16, Cleaver-Hume Press, London, 1959.
[30] G.K. Joshi, A.Y. Khot, S.R. Sawant, Solid State Commun. 65 (1988) 1593–1595.
[31] S. Deka, P.A. Joy, J. Nanosci. Nanotechnol. 8 (2008) 3955–3958.
[32] Y.F. Chen, D. Spoddig, M. Ziese, J. Phys. D: Appl. Phys. 41 (2008) 205004–205007.
[33] C.G. Koops, Phys. Rev. 83 (1951) 121–124.
[34] N. Ponpandian, A. Narayanasamy, J. Appl. Phys. 92 (2002) 2770–2778.
[35] S.J.A. Figueroa, S.J. Stewart, J. Synchrotron Radiat. 16 (2009) 63–68.
[36] M. Mozaffari, M. Eghbali Arani, J. Amighian, J. Magn. Magn. Mater. 322 (2010) 3240–3244.
[37] R. Satyanarayana, S. Ramana Murthy, T. Seshagiri Rao, J. Less-Common Met. 90 (1983) 243–250.
[38] E.J.W. Verwey, E.L. Heilmann, J. Chem. Phys. 15 (1947) 174–180.